

## Simulation of lamb wave excitation for different elastic properties and acoustic emission source geometries

Markus G. R. Sause, Siegfried R. Horn

### Angaben zur Veröffentlichung / Publication details:

Sause, Markus G. R., and Siegfried R. Horn. 2010. "Simulation of lamb wave excitation for different elastic properties and acoustic emission source geometries." *Journal of Acoustic Emission* 28: 142-54.  
<https://www.ndt.net/search/docs.php3?id=10832>.

### Nutzungsbedingungen / Terms of use:

licgercopyright

Dieses Dokument wird unter folgenden Bedingungen zur Verfügung gestellt: / This document is made available under these conditions:

**Deutsches Urheberrecht**

Weitere Informationen finden Sie unter: / For more information see:

<https://www.uni-augsburg.de/de/organisation/bibliothek/publizieren-zitieren-archivieren/publiz/>



# SIMULATION OF LAMB WAVE EXCITATION FOR DIFFERENT ELASTIC PROPERTIES AND ACOUSTIC EMISSION SOURCE GEOMETRIES

MARKUS G. R. SAUSE and SIEGFRIED HORN

University of Augsburg, Institute for Physics, Experimentalphysik II,  
D-86135 Augsburg, Germany

## Abstract

In the present study the influence of microscopic elastic properties and the geometry of the acoustic emission (AE) source are investigated by finite element simulation. We investigate the formation process of Lamb waves in isotropic and anisotropic plate specimen by simulation of five different AE source configurations. As reference a microscopically and macroscopically homogeneous, isotropic aluminum specimen with point force couples is used. For fiber-reinforced materials, the elastic properties are typically anisotropic. A comparison is made between the Lamb wave formation of the anisotropic, homogeneous model specimen and those of an anisotropic, microscopically inhomogeneous model. It is demonstrated, that the microscopic elastic properties of the AE source have significant influence on the excitation of distinct Lamb wave modes. This can be used to distinguish between failure mechanisms like fiber breakage or resin fracture in fiber reinforced materials.

## 1. Introduction

Analytical descriptions of AE sources due to crack formation and propagation and the subsequent propagation of ultrasonic signals are well established in literature [Ohtsu1984, Giordano1999, Lysak1996]. Based on the generalized theory of AE, the microscopic crack surface displacement can be linked to the macroscopic displacement at the surface of the solid by suitable Green's functions [Ohtsu1986]. While the Green's functions for partially infinite media are easy to obtain, the situation grows more difficult, when dealing with complex geometries of finite extent. In addition, another major difficulty is the application of Green's functions to inhomogeneous, anisotropic media. Although such cases can be investigated by analytical descriptions [Green1995, Green1998], they are typically only suited for the specific geometry and material under investigation.

In recent years various authors have applied the finite element method (FEM) to the simulation of AE formation and AE signal propagation for the case of plate specimens [Dietzhausen1998, Prosser1999, Hamstad2002]. The AE source was typically modeled as point force couple. Due to the increase in computational capacities such simulations are becoming an important part to improve the understanding of AE signal formation and propagation.

The finite element method allows an intuitive approach to subdivide modeling and simulation of AE signals. Utilizing a multi-scale approach the modeling of AE can be split into three distinct steps:

- Modeling of source mechanism
- Modeling of signal propagation
- Modeling of signal detection

The first step addresses the description of the AE source. Typically buried dipole sources realized as point force couples are used. This requires knowledge of the source radiation direction

and the associated magnitudes of the modeled source mechanism. In addition, various source-time functions are employed in literature, which model the source kinematics [Ohtsu1986, Giordano1999, Hamstad1999]. In a previous publication, we presented a new source model to simulate the microscopic failure in carbon-fiber reinforced plastics (CFRP). This source model takes into account the finite extent of the crack and the microscopic geometry and elastic properties of the AE source [Sause2010]. Thus in the following the term “source model” refers to the finite dimensions of the crack model and the geometry and elastic properties in the vicinity of the crack model.

Subsequent to signal excitation, the elastic wave propagates into the solid and is reflected at the respective boundaries of the geometry. In plate-like geometries with thickness  $d$  the signal propagation is analytically described by Lamb waves for wavelengths  $\lambda < 3d$  [Lamb1917]. In finite element simulations the propagation of such signals is modeled based on time dependent solutions of differential equations of the equilibrium states [Castaings2004, Nieuwenhuis2005, Prosser1999, Hamstad1999, Sause2010]. As pointed out for isotropic media by Hamstad et al., different source radiation directions can excite different ratios of symmetric and antisymmetric Lamb wave modes [Hamstad2002]. This in turn can lead to different frequency compositions of the detected AE signals, as the propagation of the zero-order symmetric ( $S_0$ ) mode occurs at higher frequency than the zero-order antisymmetric ( $A_0$ ) mode [Hamstad2002]. Due to the microscopically inhomogeneous nature of fiber-reinforced composites, strong differences in the source radiation direction are expected depending on the failure mechanism. In a previous publication it was demonstrated, that such differences of the source radiation direction and of the microscopic elastic properties cause distinct differences in the excited Lamb wave modes, which compare well to experimental data recorded during failure of CFRP specimens [Sause2010, Sause2010b]. In addition, influences of the displacement magnitude and the source excitation time were investigated [Sause2010].

Signal propagation in the previously used specimen types suffered drastically from boundary reflections [Sause2010, Sause2010b], since interference of signals with their boundary reflections makes identification of distinct Lamb wave modes more difficult. Therefore, this approach is extended to larger specimen geometries. In addition, the case of isotropic media is treated as a reference.

Finally, the importance of simulation of the detection process of AE signals cannot be over-emphasized. While in [Sause2010] an abstract representation of a typical broadband piezoelectric sensor was used, this approach was extended to a full-scale simulation in [Sause2010b]. However, since the present study will focus on basic investigation of the influence of the source microstructure the detection process will be limited to the simulation of surface displacements at distinct positions at the model specimen surface.

## 2. Description of Model

The present simulations were performed for rectangular plate specimens with 200 mm x 400 mm edge length and 1.4 mm thickness. Utilizing symmetric boundary conditions at the yz- and xz-plane only one quarter of the total plate volume was modeled as shown in Fig. 1. The AE source is located at the medial plane at the center of the plate specimen  $(x,y,z) = (0,0,0)$  mm. All elastic properties describing the propagation medium and the source model are summarized in Table 1. The respective AE signals are obtained from the surface displacements at the positions marked in Fig. 1 (red crosses) under an angle  $\theta$ .

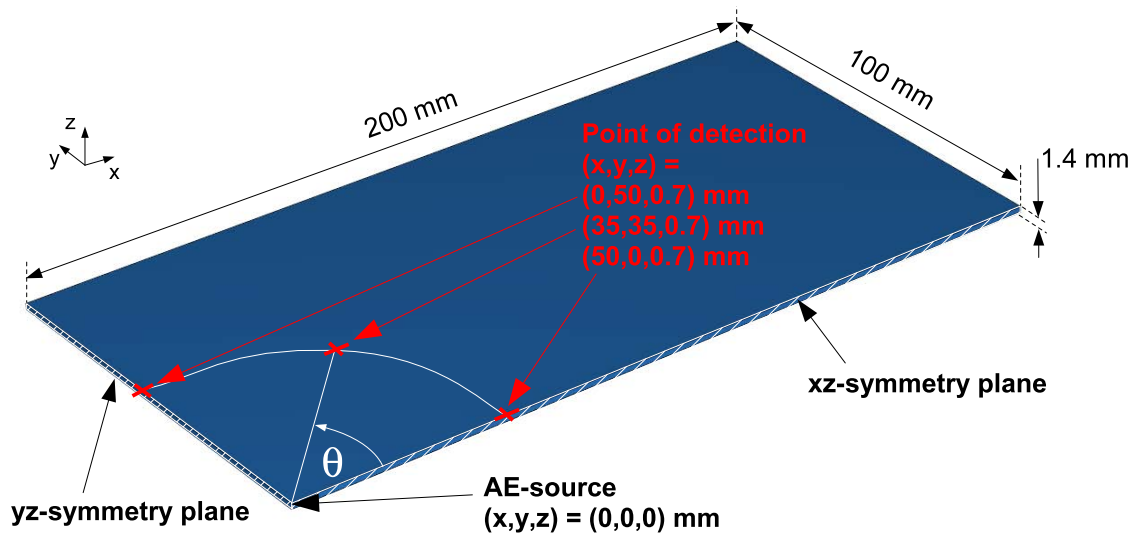


Fig. 1: Schematic drawing of plate model including dimensions and symmetry planes.

Table 1: Summary of elastic properties of the materials used within the simulation.

	<b>Aluminum 6063-T83</b>	<b>CFRP T800/913</b>	<b>Resin HexPly 913</b>	<b>Carbon Fiber T800S</b>
Density [kg/m <sup>3</sup> ]	2700	1550	1230	1810
Poisson-Ratio	0.33	-	0.35	0.20
Elastic coefficients [GPa]	E = 69.0	C <sub>11</sub> = 154.0 C <sub>12</sub> = 3.7 C <sub>13</sub> = 3.7 C <sub>22</sub> = 9.5 C <sub>23</sub> = 5.2 C <sub>33</sub> = 9.5 C <sub>44</sub> = 2.5 C <sub>55</sub> = 4.2 C <sub>66</sub> = 4.2	E = 3.39	E = 294.0

A quarter-volume representation of the various microscopic source models is shown in Fig. 2-a-f. Five different configurations of source models were used in the following:

- (A) Isotropic aluminum plate and homogeneous source
- (B) Anisotropic CFRP plate and homogeneous source
- (C) Anisotropic CFRP plate and inhomogeneous source (resin properties)
- (D) Anisotropic CFRP plate and inhomogeneous source (carbon fiber properties)
- (E) Point force couple

The first configuration is shown in Fig. 2-a. The crack is modeled as a three-axes cross, which is cut out of the homogeneous medium around the source. Each of the three axes of the cross is composed of a bar of 30- $\mu$ m length, and 10  $\mu$ m x 10  $\mu$ m cross-section, respectively. The remaining domains visible in Fig. 2-a are not relevant for this case and will be explained below. For the present configuration, all domains were assigned elastic properties of aluminum. The second configuration is also represented by Fig. 2-a, although all domains were now assigned

homogeneous, anisotropic elastic properties of T800/913. The third configuration is shown in Fig. 2-b. Here the microscopic elastic properties of a cube with edge length  $r_{cube} = 200 \mu\text{m}$  were those of the HexPly 913 resin as given in Table 1. The elastic properties of the macroscopic plate were those of T800/913. While the dimensions of the crack model and the remaining domains were all comparable to the configurations considered before, now a smooth transition between microscopic and macroscopic elastic properties is required. This is achieved utilizing a cube with  $2r_{cube} = 400 \mu\text{m}$  edge length which encloses the resin cube. This so-called perfectly matched layer (PML) gradually changes the elastic properties of the enclosed medium  $C_{ij,0}$  to those of the surrounding medium  $C_{ij,1}$  as a function of distance  $r$  as follows:

$$C'_{ij} = \begin{cases} C_{ij,0} & r < r_{cube} \\ C_{ij,0} + \left( \left( \frac{r}{r_{cube}} - 1 \right) \cdot (C_{ij,1} - C_{ij,0}) \right) & r_{cube} \leq r \leq 2r_{cube} \\ C_{ij,1} & r > 2r_{cube} \end{cases} \quad (1)$$

The material density was gradually changed accordingly. This smooth transition is exemplarily visualized in Fig. 2-d in a pseudo-color diagram. The fourth source model configuration differs from the third configuration only by a different assignment of elastic properties of the domain marked in red in Fig. 2-c. In this case the cuboid with edge length of  $85 \mu\text{m}$  and  $10 \mu\text{m} \times 10 \mu\text{m}$  cross-section has elastic properties of T800S carbon fibers instead of HexPly913 resin. The respective transition to the macroscopic properties of the T800/913 CFRP plate is realized by a respective PML as shown in Fig. 2-e. For the purpose of comparison, point force couples as shown in Fig. 2-f were also simulated. In the present configuration, the total distance of the two points acting as buried dipole source was  $300 \mu\text{m}$  with  $1 \text{ N}$  force magnitude.

In order to excite an AE signal, in the following a linear source-time function was used. Since the influence of various source radiation directions was already addressed in [Sause2010], in the present study only in-plane crack surface displacements  $d_x$  as marked in Fig. 2-b were considered. Following the previous publications, a linear source-time function was used to deflect the respective crack surface by a magnitude  $d_{0,x}$  within an excitation time  $T_{e,x}$  [Sause2010, Sause2010b]:

$$d_x(t) = \begin{cases} d_{0,x} \cdot \left( \frac{t}{T_{e,x}} \right) & 0 \leq t \leq T_{e,x} \\ free & t > T_{e,x} \end{cases} \quad (2)$$

After the excitation time  $T_{e,x}$ , the boundaries of the source model are free of constraints. The subscript  $x$  marks the respective direction of crack surface deflection. It is worth to note that due to the symmetry conditions of the model the crack surface displacement is also symmetrical with respect to the  $yz$ -plane. For better comparison of the obtained results, the magnitude  $d_{0,x}$  and excitation time  $T_{e,x}$  was kept constant for all models at  $d_{0,x} = 100 \text{ nm}$  and  $T_{e,x} = 100 \text{ ns}$ .

Since the present approach introduces a multi-scale problem, the resolution of the finite element mesh was gradually refined from  $2.0 \text{ mm}$  down to  $0.01 \text{ mm}$  when approaching the model source. The higher mesh resolution close to the source is necessary to resolve the geometric details of the source model, while the coarse macroscopic resolution is still sufficient to describe signal propagation within the plate specimen up to frequencies of  $1 \text{ MHz}$ . Since exact symmetry and quality of arbitrarily generated 3D tetrahedral meshes is typically difficult to achieve [Fritag1997, Parthasarathy1994], the source model could not be meshed symmetrically with respect to the  $xy$ -plane.

Consequently, there is a break of symmetry with respect to the  $xy$ -plane, which can cause differences in the calculation of signal propagation along the positive and negative direction of the  $z$ -axis, respectively. As a result antisymmetric Lamb wave modes can occur. The sensitivity of the Lamb wave formation based on this effect cannot be overemphasized. Within reasonable steps of refinement of the mesh density around the source model the excitation of antisymmetric Lamb waves could not be prevented. Based on physical considerations such microscopic asymmetry within the material is always expected and therefore the present configuration is meant to reflect realistic conditions better than perfect symmetric mesh conditions. To ensure comparability of the results of different source model configurations, in the following all simulations were performed using an identical mesh.

The temporal resolution was chosen to be 10 ns for  $t < 1 \mu\text{s}$ , which is required to resolve the excitation process. For  $1 \mu\text{s} \leq t \leq 50 \mu\text{s}$  the temporal resolution was decreased to 100 ns, which is sufficient to temporally resolve the signal propagation process.

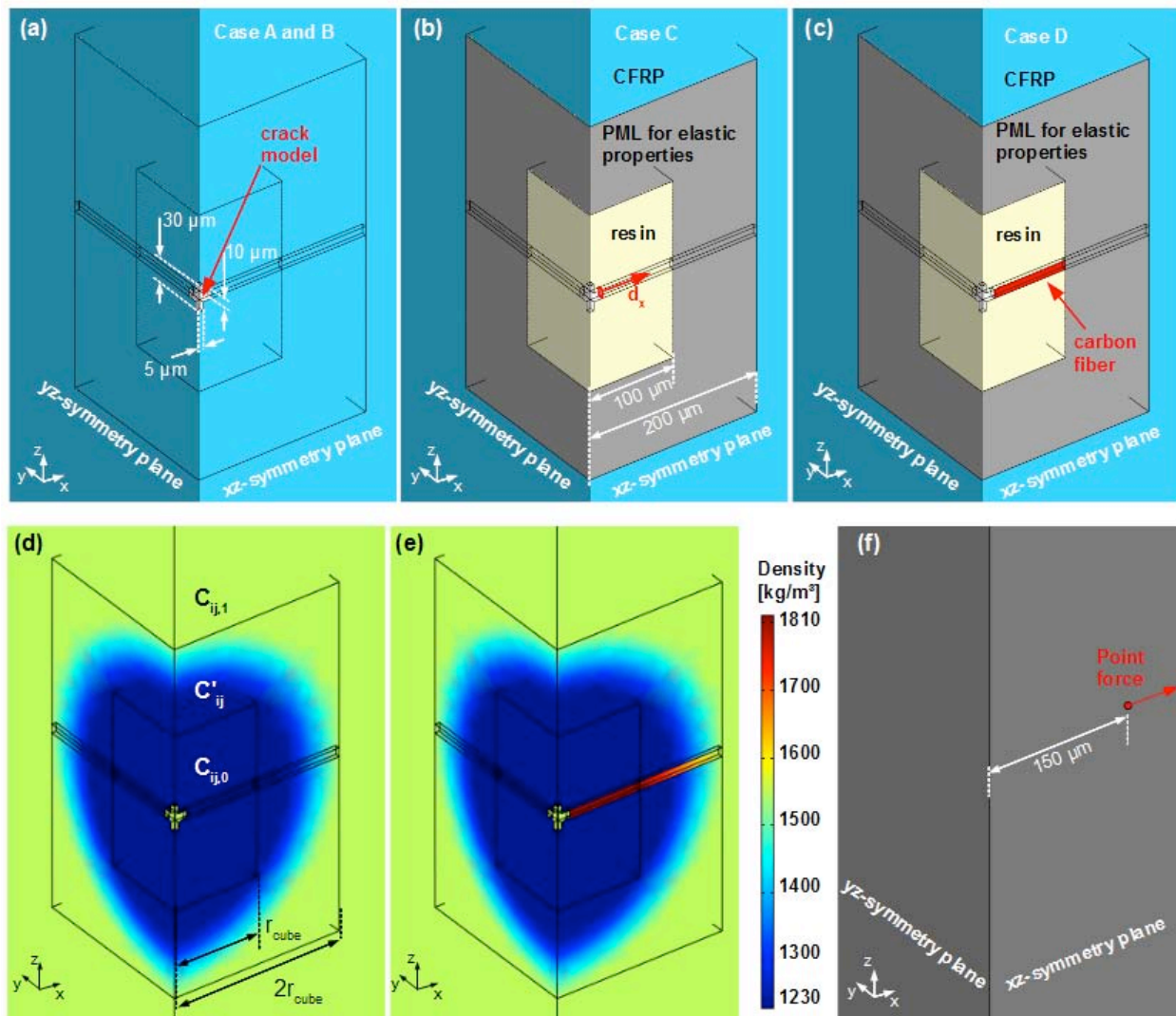


Fig. 2: Quarter-volume representation of AE source model configurations. (a) Homogeneous case. (b) model of matrix cracking. (c) model of fiber breakage. (d, e) Pseudo-color diagram of material density visualizes transition of elastic properties utilizing perfectly matched layer and (f) model of point force couple.

### 3. Results

The results of the simulations are presented below for the five different source model configurations. To visualize the modal composition of the AE signals the Choi-Williams transformation is calculated using the software package AGU-Vallen Wavelet [Choi1989, Vallen2010]. The results are compared to analytical solutions of dispersion curves calculated for the respective propagation medium and distance [Vallen2010, Zeyde2010].

#### 3.1 Homogeneous, isotropic medium

The Lamb wave propagation excited by source model configuration A is shown in Fig. 3 at six distinct times. The in-plane displacement located at the medial plane of the plate excites a strong  $S_0$  Lamb wave mode with preferential orientation along the x-axis. As visible in Fig. 3, for  $35 \mu\text{s} < t < 50 \mu\text{s}$  minor reflections occur at the boundary in y-direction. But for times  $t < 40 \mu\text{s}$  no boundary reflections arrive at the designated detection positions.

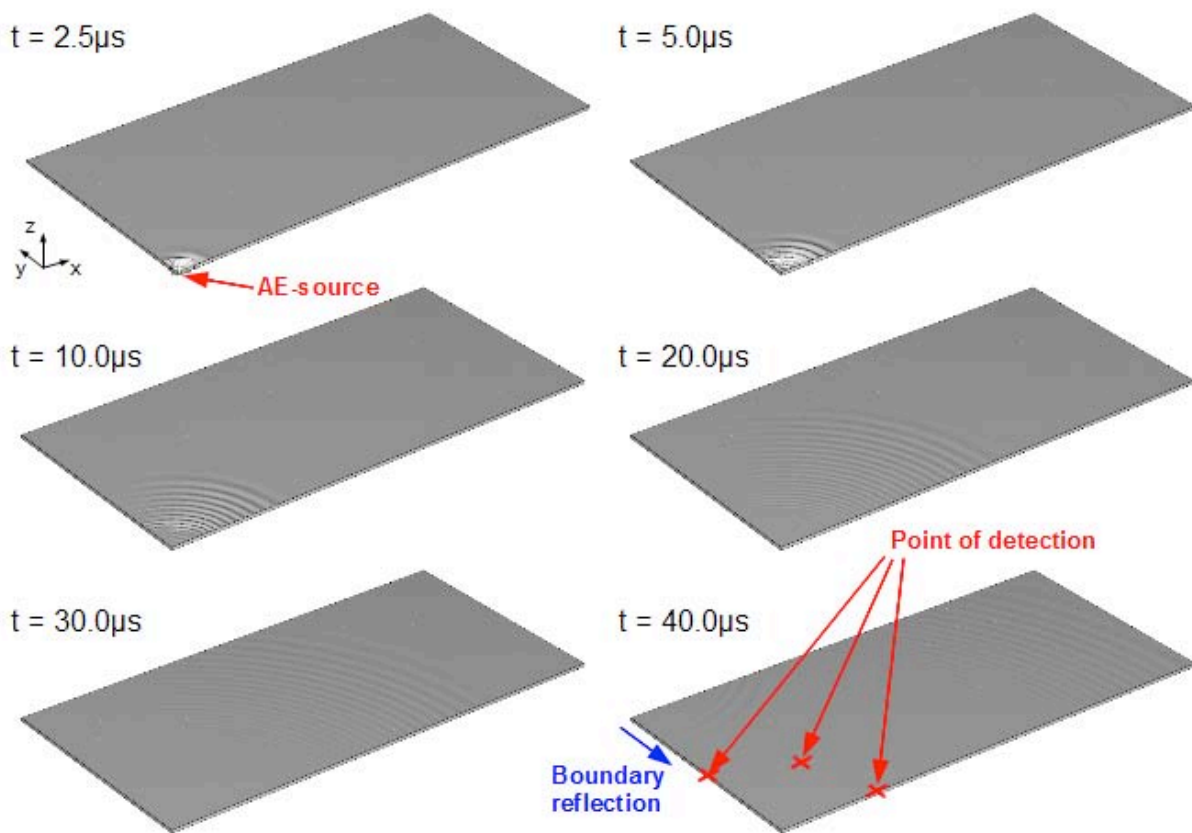


Fig. 3: Propagation of  $S_0$  Lamb wave mode in aluminum plate at six distinct times.

As already mentioned in the introduction section, point force couples are often used in literature to model AE sources. Following the approach of Hamstad et al. [Hamstad1999] a respective aluminum plate with dimensions as given in Fig. 1 was modeled, using an in-plane point force couple. The resulting CWD-diagram of the z-displacement of the surface at  $(x,y,z) = (50,0,0.7)$  mm is shown in Fig. 4-a. For comparison the CWD-diagram of the signal at the respective position using the source model configuration A is shown in Fig. 4-b. In addition both CWD-diagrams show dispersion curves for the  $S_0$  and  $A_0$  Lamb wave modes calculated for the propagation distance of 50 mm. For aluminum with elastic properties as given in Table 1, the

longitudinal and transversal wave velocities were calculated as  $v_L = 6153$  m/s and  $v_T = 3100$  m/s, respectively.

Clearly, the signals of both simulations are dominated by the contribution of the  $S_0$  Lamb wave mode as seen in Fig. 3. In direct comparison the source model configuration of finite extent shows in addition an excitation of the  $A_0$  Lamb wave mode. This contribution is hardly visible in the CWD-diagram in Fig. 4, since the magnitude of the coefficients is dominated by the intensity of the  $S_0$  Lamb wave mode. Instead, the minor contribution of the  $A_0$  Lamb wave mode is observed better as low frequency oscillation of the signal in time domain after  $t = 13$   $\mu$ s.

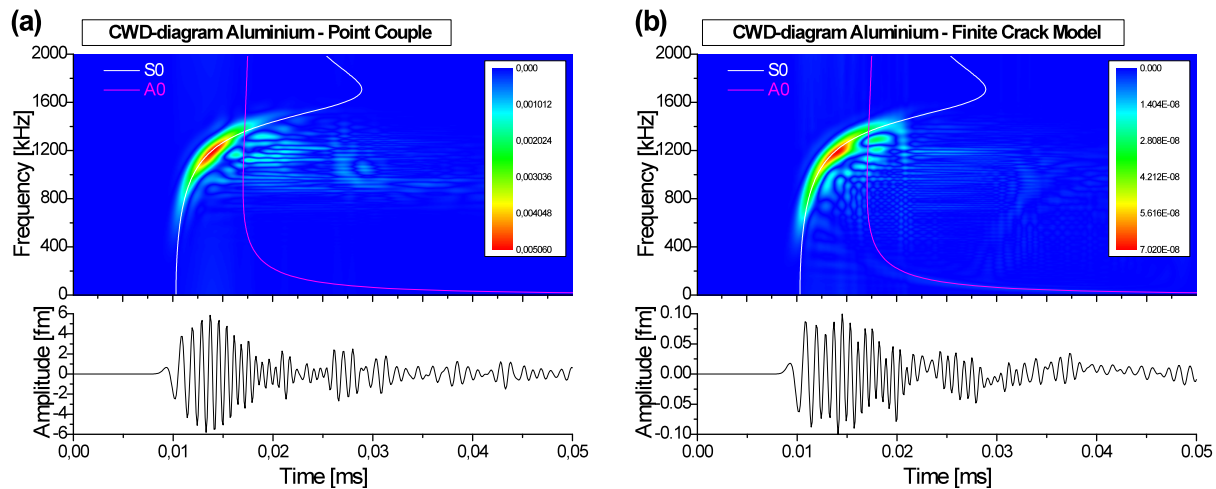


Fig. 4: Comparison of surface displacement signals at  $(x,y,z) = (50,0,0.7)$  mm for point force couple model (a) and model of finite extent (b) with superimposed dispersion curves.

Since the source model configuration A uses an axially oriented surface displacement, a dependency on the orientation of the source relative to the sensor can be expected. As depicted in Fig. 1 the surface displacement signals were detected at three distinct points, reflecting three different source-sensor angles of  $\theta = 0^\circ$ ,  $45^\circ$  and  $90^\circ$ , respectively, between the crack surface normal ( $x$ -axis) and the investigated propagation direction.

The CWD-diagrams in Fig. 5 show the respective simulated signals for the source model configuration A with additionally calculated dispersion curves. Clearly, the modal composition of the detected Lamb waves depends on the angle. While for the source-sensor angle  $0^\circ$  the  $S_0$  mode dominates, the  $S_0$  mode contribution decreases for  $45^\circ$  and vanishes for  $90^\circ$ . In contrast, the contribution of the  $A_0$  Lamb wave mode is almost constant for all three angles, although barely visible in the color-range of Fig. 5-a. Due to the orientation of the in-plane crack surface displacement, this preferential spatial distribution of the  $S_0$  mode intensity is expected [Eaton2008].

### 3.2 Homogeneous, anisotropic medium

The Lamb wave propagation excited by source model configuration B is visible in Fig. 6. Generally, the propagation of Lamb waves in anisotropic media like CFRP is more complex than for isotropic media. Due to the elastic anisotropy, the propagation of distinct Lamb wave modes is strictly asymmetric. Due to the high elastic modulus in  $x$ -direction (154 GPa) the propagation velocity of the  $S_0$  Lamb wave mode along the  $x$ -axis is very high and thus the reflection at the  $x$ -edge of the specimen interferes at the observation position  $(x,y,z) = (50,0,0.7)$  mm for  $t > 35$   $\mu$ s.

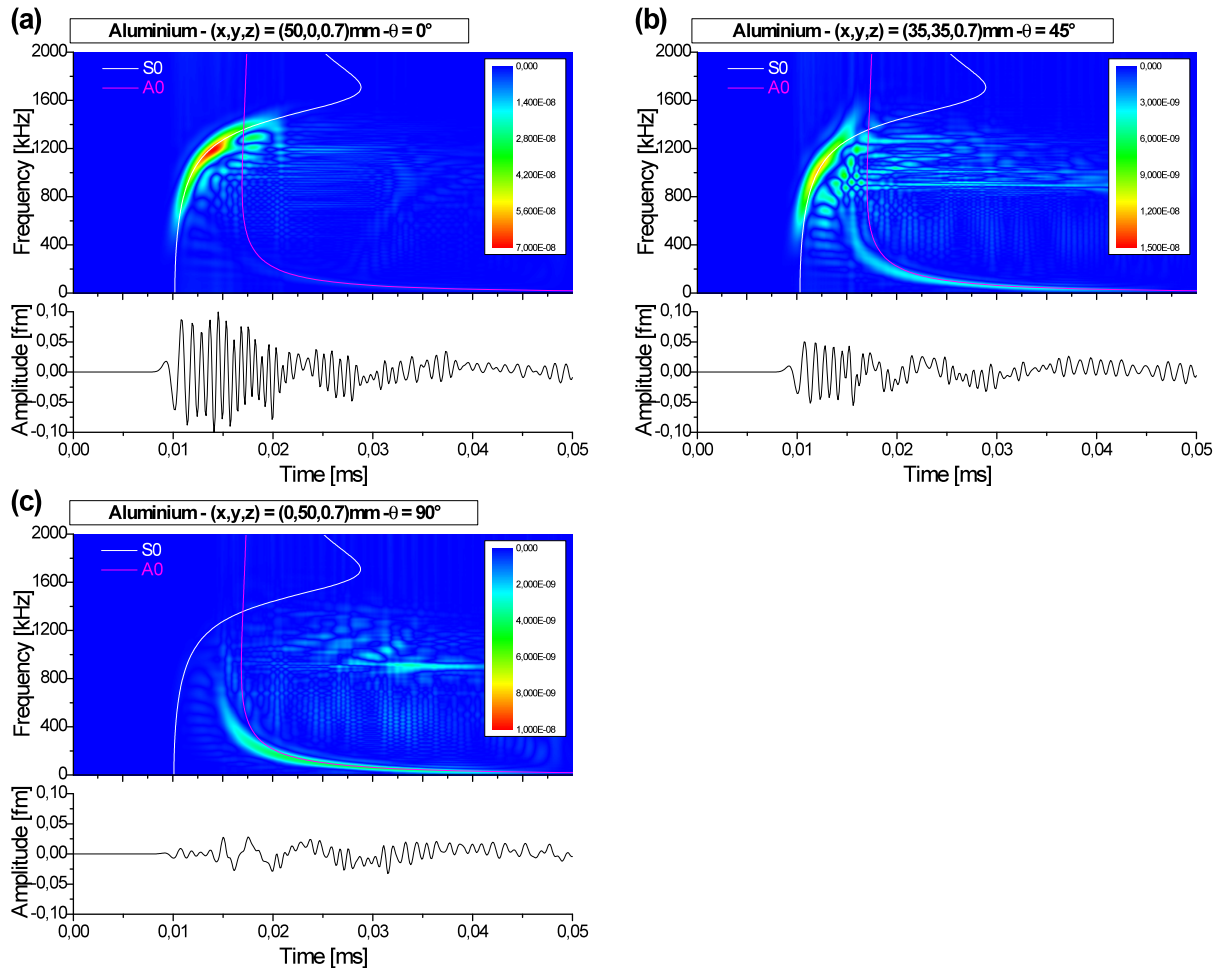


Fig. 5: Influence of source-sensor angle for source model configuration A: (a) at  $(x,y,z) = (50,0,0.7)$  mm, (b)  $(x,y,z) = (35,35,0.7)$  mm, (c)  $(x,y,z) = (0,50,0.7)$  mm.

However, the other observation positions marked in Fig. 6 show no interference with incident reflections for the investigated time  $t < 50 \mu\text{s}$ .

In analogy to the case of isotropic media considered before, a comparison is made between signals excited by point force couples in an anisotropic plate and those of source model configuration B. The resulting CWD-diagrams of the z-displacement signal of the surface at  $(x,y,z) = (50,0,0.7)$  mm are shown in Fig. 7-a and 7-b. In addition, dispersion curves of the S<sub>0</sub> and A<sub>0</sub> Lamb wave modes are shown. Both were calculated for propagation in x-direction based on the anisotropic elastic properties given in Table 1 using the software package of R. Zeyde [Zeyde2010]. As visible in Fig. 7, both signals are clearly dominated by the S<sub>0</sub> Lamb wave mode.

### 3.3 Inhomogeneous, anisotropic medium

After introducing an anisotropic propagation medium and AE sources of finite dimensions in source models A and B, the source model configurations C and D introduce microscopic inhomogeneous elastic properties. These are used to model the microscopic presence of resin and carbon fibers as shown in Fig. 2-b and 2-c. A comparison of CWD-diagrams of both source model configurations is shown in Fig. 8 for each source-sensor angle investigated. In addition, the dispersion curves of the fundamental Lamb wave modes are shown in each CWD-diagram.

These were calculated independently for each source-sensor angle and the respective propagation distance using the software package of Zeyde [Zeyde2010].

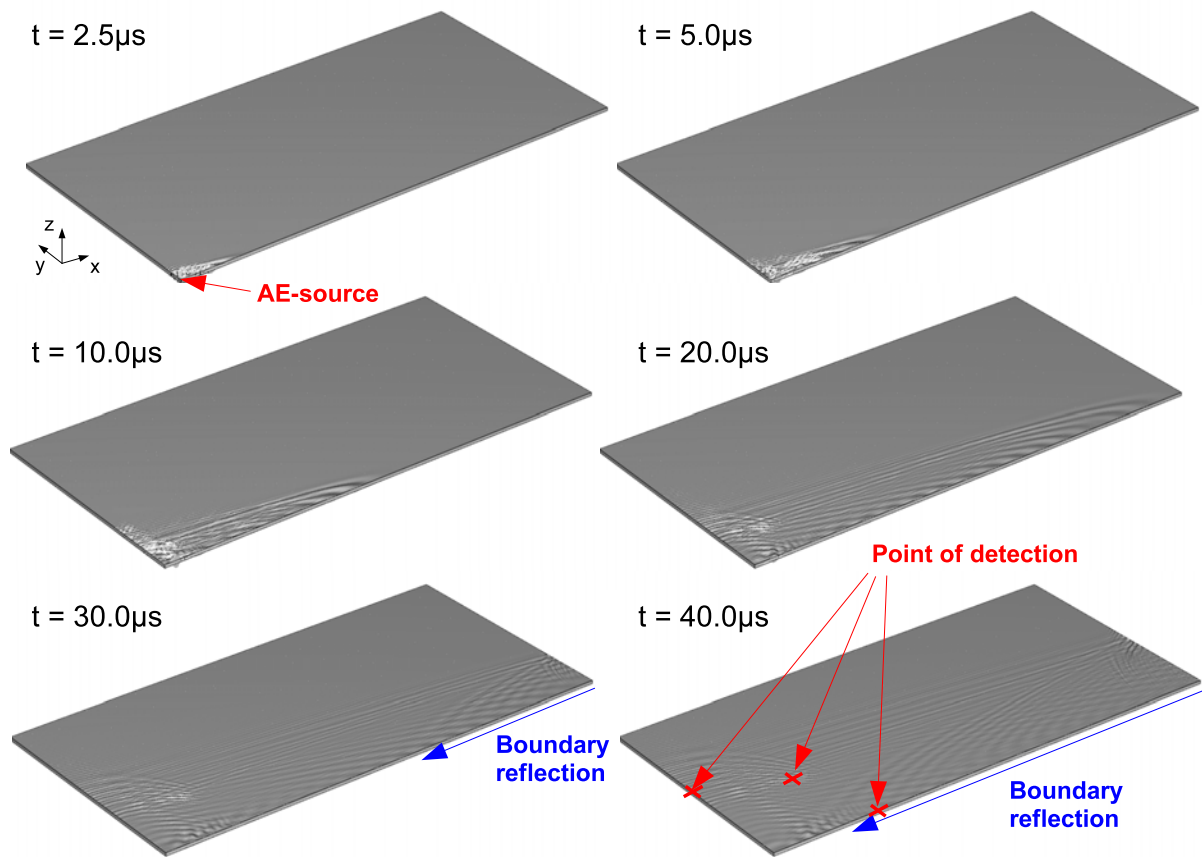


Fig. 6: Propagation of several Lamb wave modes in CFRP plate at six distinct times.

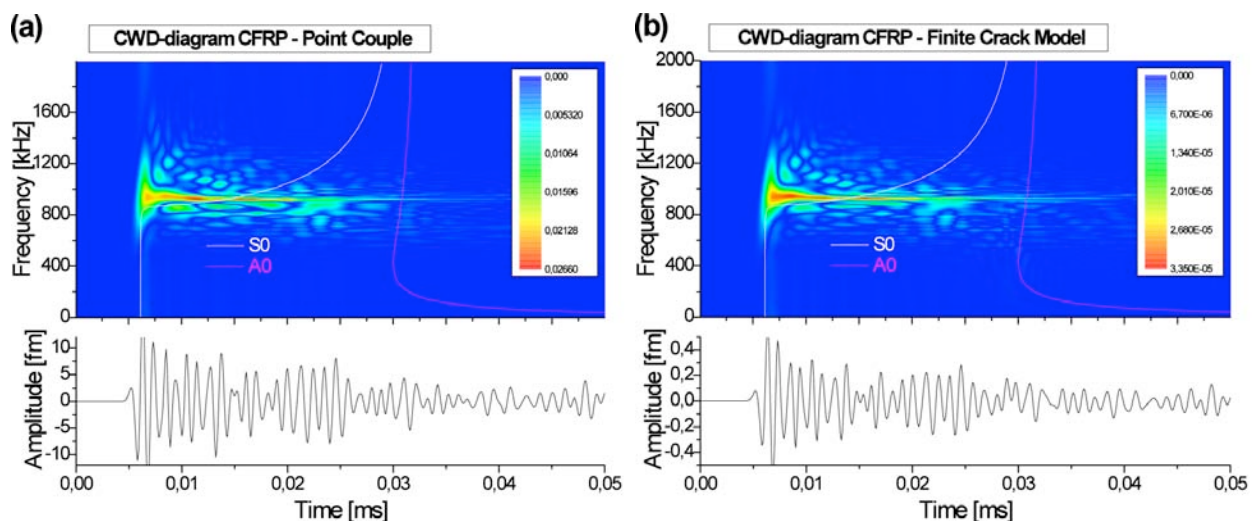


Fig. 7: Comparison of surface displacement signals at  $(x,y,z) = (50,0,0.7)$  mm for point force couple model (a) and model of finite extent (b) with superimposed dispersion curves.

For source model configuration C (model of matrix cracking), the signals are dominated by the  $A_0$  mode for all source-sensor angles (see Fig. 8a-c). Only minor contributions of the  $S_0$  Lamb wave modes are observed. These are barely visible in the CWD-diagrams, but are easier to

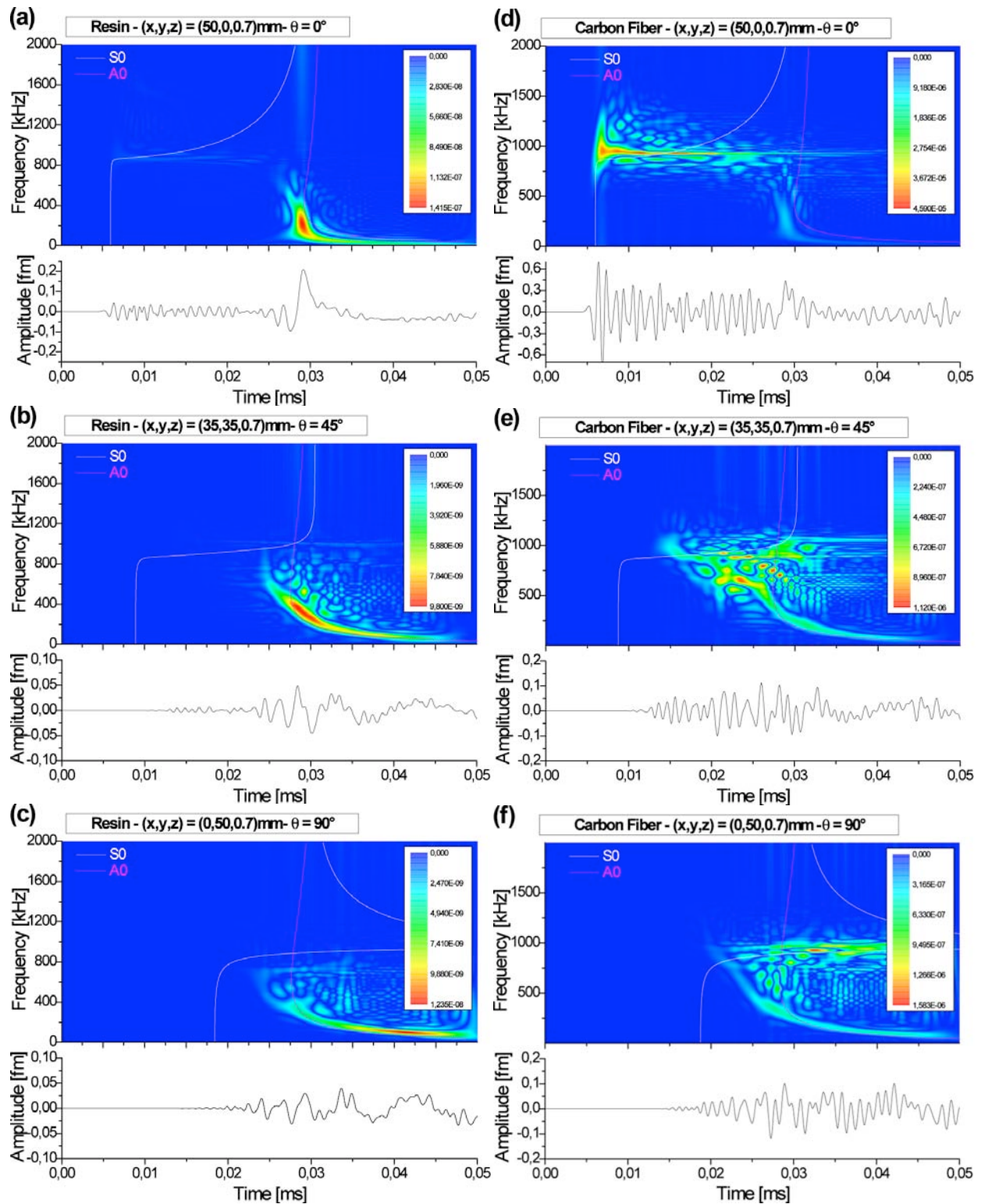


Fig. 8: Influence of source-sensor angle for source model configuration C (a) at  $(x, y, z) = (50, 0, 0.7)$  mm, (b)  $(x, y, z) = (35, 35, 0.7)$  mm, (c)  $(x, y, z) = (0, 50, 0.7)$  mm and (d – f) for source model configuration D, respectively.

identify in the time domain at the beginning of the signals, in particular for observation position  $(x, y, z) = (50, 0, 0.7)$ .

Different CWD-diagrams are observed for source model configuration D (model of fiber breakage) at the respective observation positions. Here a strong contribution of the  $S_0$  Lamb wave mode is found for propagation direction parallel to the crack surface normal (see Fig. 8-d). With increasing source-sensor angle, the contribution of the  $S_0$  mode decreases, since it is directed mostly along the x-axis as seen in Fig. 6. Thus the dominant contribution for  $(x,y,z) = (35,35,0.7)$  mm and  $(x,y,z) = (0,50,0.7)$  mm originates from the  $A_0$  mode.

It is worth pointing out that the same source excitation time was used in the current simulations for both source model configurations. Based on the transversal sound velocity, the source excitation time of fiber breakage is expected to be shorter than for resin fracture. As already presented in [Sause2010] this results in a stronger contribution of the intensity of the  $S_0$  mode for the case of fiber breakage and, consequently, emphasizes the characteristic difference between the associated source mechanisms further.

#### 4. Conclusions

For isotropic media the results of conventional point force couples and of the source model of finite extent as introduced in [Sause2010] agree reasonably well. For the source model of finite extent a weak additional contribution of the  $A_0$  Lamb wave mode is found, which is attributed to the influence of asymmetry of the used tetrahedral mesh on a microscopic scale. Although the asymmetry was introduced accidentally, it is expected to reflect real experimental conditions better than symmetric meshes, since minor deviations from perfect symmetry in the form of voids and flaws will always be present. Due to the fact that the dimensions of these inhomogeneities are within the range of the wavelengths occurring close to the source they will strongly affect the symmetry of the source radiation patterns.

Independent of the chosen mesh, for the investigated source model configurations in anisotropic media a strong influence of the microscopic elastic properties on the modal composition of the excited Lamb waves was found. In this context it was demonstrated, that just the change of local elastic properties from those of resin to those of carbon fiber cause a different excitation ratio of symmetric and antisymmetric Lamb wave modes.

In all specimens a strong dependency of the signal propagation on the orientation between the axis normal to crack surface displacement and the source-sensor axis was found. For isotropic media the orientation of the in-plane source causes a preferential orientation of the  $S_0$  mode propagation along the direction of the crack surface normal. A superposition of the calculated fundamental Lamb wave modes shows good agreement to simulated signals.

Since for anisotropic media the dispersive propagation of Lamb waves depends on the direction, different dispersion curves were calculated for the investigated propagation angles of  $0^\circ$ ,  $45^\circ$  and  $90^\circ$ . Similar to the isotropic propagation medium, the  $S_0$  mode propagates with preferential orientation along the direction of the crack surface normal. For the current model this direction coincides with the fiber axes and thus results in a fast propagation of the  $S_0$  mode. For the purpose of source identification procedures, this dependency of Lamb wave propagation on the source-sensor angle introduces additional difficulties. For a valid identification of the microscopic source mechanism this effect has to be taken into account.

For further investigations of the effect of the source microstructure the geometry of the presented source model should be extended. In order to model typical failure mechanisms in CFRP, the influence of the vicinity of the source should be investigated in more detail. In particular, a more realistic crack geometry should be considered. The influence of inhomogeneities, like additional fibers and voids in the surrounding of the source should be investigated. In addition, the influence of fiber-matrix interfacial strength is not taken into account in the current model. In future attempts, this interaction should be treated accordingly.

For signals detected at distances below 50 mm, geometric spreading is the dominating contribution to attenuation. To interpret signals at longer propagation distances additional contributions to Lamb wave attenuation should be taken into account by modeling of dispersive media.

In summary, the presented simulations demonstrate that the microscopic conditions close to the source influence the excitation of distinct Lamb wave modes significantly. For experimental attempts regarding source identification procedures, such influences should be taken into account, since they can dominate the signal characteristics and thus superimpose effects of dispersive signal propagation.

## Acknowledgments

We like to thank Professor M. Hamstad for valuable suggestions regarding simulation of acoustic emission.

## References

- [Castaings, 2004] M. Castaings, C. Bacon, B. Hosten and M.V. Predoi, "Finite element predictions for the dynamic response of thermo-viscoelastic material structures", *Journal of the Acoustic Society of America*, **115** (3), 1125-1133 (2004).
- [Choi, 1989] H.-I. Choi and W. Williams, "Improved Time-Frequency Representation of Multicomponent Signals Using Exponential Kernels", *IEEE Transactions on Acoustics, Speech and Signal Processing*, **37** (6), 862-872 (1989).
- [Dietzhausen, 1998] H. Dietzhausen, M. Dong and S. Schmauder, "Numerical simulation of acoustic emission in fiber reinforced polymers", *Computational Materials Science*, **13**, 23-30 (1998).
- [Eaton, 2008] M.J. Eaton, R. Oullin, K.M. Holford and C.A. Featherston, "AE wave propagation and novel source location in composite plates", 28<sup>th</sup> European Conference on AE Testing, Krakow, Poland (2008)
- [Freitag, 1997] L.A. Freitag and C. Ollivier-Gooch, "Tetrahedral mesh improvement using swapping and smoothing", *Numerical Methods in Engineering*, **40** (21), 3979-4002 (1997)
- [Giordano, 1999] M. Giordano, L. Condelli and L. Nicolais, "Acoustic emission wave propagation in a viscoelastic plate", *Composites Science and Technology*, **59**, 1735-1743 (1999).
- [Green, 1995] E. R. Green, "Acoustic emission sources in a cross-ply laminated plate", *Composites Engineering*, **5**, 1453-1469 (1995).
- [Green, 1998] E.R. Green, "Acoustic Emission in Composite Laminates", *Journal of Nondestructive Evaluation*, **17** (3), 117-127 (1998).

- [Hamstad, 2002] M.A. Hamstad, A. O’Gallagher and J. Gary, “A Wavelet Transform Applied To Acoustic Emission Signals: Part 1: Source Identification”, *Journal of Acoustic Emission*, **20**, 39-61 (2002).
- [Hamstad, 1999] M.A. Hamstad, A. O’Gallagher and J. Gary, "Modeling of Buried Acoustic Emission Monopole and Dipole Sources With a Finite Element Technique", *Journal of Acoustic Emission*, **17** (3-4), 97-110 (1999).
- [Lamb, 1917] H. Lamb. “On Waves in an Elastic Plate”, *Proceedings of the Royal Society of London Series A, Containing Papers of a Mathematical and Physical Character*, **93**, 114-128 (1917).
- [Lysak, 1996] M. Lysak. “Development of the theory of acoustic emission by propagating cracks in terms of fracture mechanics”, *Engineering Fracture Mechanics*, **55** (3), 443-452 (1996).
- [Nieuwenhuis, 2005] J.H. Nieuwenhuis, J. Neumann, D.W. Greve and I.J. Oppenheim, “Generation and detection of guided waves using PZT wafer transducers”, *IEEE Transactions Ultrasonics, Ferroelectrics and Frequency Control*, **52**, 2103-2111 (2005).
- [Ohtsu, 1984] M. Ohtsu and K. Ono, “A generalized theory of acoustic emission and Green's function in a half space”, *Journal of Acoustic Emission*, **3**, 27-40 (1984).
- [Ohtsu, 1986] M. Ohtsu and K. Ono, “The generalized theory and source representation of acoustic emission”, *Journal of Acoustic Emission*, **5**, 124-133 (1986).
- [Parthasarathy, 1994] V.N. Parthasarathy, C.M. Graichen and A.F. Hathaway, “A comparison of tetrahedron quality measures”, *Finite Elements in Analysis and Design*, **15** (3), 255-261 (1994).
- [Prosser, 1999] W.H. Prosser, M.A. Hamstad, J. Gary and A. O’Gallagher, “Finite Element and Plate Theory Modeling of Acoustic Emission Waveforms”, *Journal of Nondestructive Evaluation*, **18** (3), 83-90 (1999).
- [Sause, 2010] M.G.R. Sause and S. Horn, “Simulation of acoustic emission in planar carbon fiber reinforced plastic specimens”, *Journal of Nondestructive Evaluation*, **29** (2), 123-142 (2010).
- [Sause, 2010b] Markus G.R. Sause and Siegfried Horn, “Influence of Specimen Geometry on Acoustic Emission Signals in Fiber Reinforced Composites: FEM-Simulations and Experiments”, *Conference Proceedings: 29th European Conference on Acoustic Emission Testing*, Vienna, Austria (2010).
- [Vallen, 2010] Vallen Systeme GmbH (Munich, Germany), Aoyama Gakuin University (Tokyo, Japan). AGU-Vallen Wavelet (2010).
- [Zeyde, 2010] R. Zeyde, “Notes on orthotropic Lamb waves”, Technion - Israel Institute of Technology, <http://mercurial.intuxication.org/hg/elasticssim/> (2010).